


BRIEF REPORT



Selective inhibition of carbonic anhydrase IX and XII by coumarin and psoralen derivatives

Rita Meleddu^a , Serenella Deplano^a, Elias Maccioni^a , Francesco Ortuso^b , Filippo Cottiglia^a, Daniela Secci^a, Alessia Onali^a, Erica Sanna^a, Andrea Angeli^c , Rossella Angius^d, Stefano Alcaro^b , Claudiu T. Supuran^c  and Simona Distinto^a 

^aDepartment of Life and Environmental Sciences, University of Cagliari, Monserrato, Italy; ^bDipartimento di Scienze della Salute, Università Magna Graecia di Catanzaro, Catanzaro, Italy; ^cDipartimento NEUROFARBA, Sezione di Scienze Farmaceutiche, Università degli Studi di Firenze, Sesto Fiorentino, Italy; ^dLaboratorio NMR e Tecnologie Bioanalitiche, Sardegna Ricerche, Pula, Italy

ABSTRACT

A small library of coumarin and their psoralen analogues **EMAC10157a-b-d-g** and **EMAC10160a-b-d-g** has been designed and synthesised to investigate the effect of structural modifications on their inhibition ability and selectivity profile towards carbonic anhydrase isoforms I, II, IX, and XII. None of the new compounds exhibited activity towards hCA I and II isozymes. Conversely, both coumarin and psoralen derivatives were active against tumour associated isoforms IX and XII in the low micromolar or nanomolar range of concentration. These data further corroborate our previous findings on analogous derivatives, confirming that both coumarins and psoralens are interesting scaffolds for the design of isozyme selective hCA inhibitors.

ARTICLE HISTORY

Received 8 January 2021
Revised 27 January 2021
Accepted 1 February 2021

KEYWORDS

hCAi; tumour; coumarin; psoralen; docking

Introduction

The development of cancer is a complex multifactorial process, involving many cellular adaptations and signal transduction pathways^{1–4}. In solid tumours, cancer cells must survive in a low oxygen concentration environment, due to the rapid cellular proliferation and to the impossibility to promptly supply an adequate vascularisation^{5,6}. Indeed, many pathways are involved in the hypoxia survival mechanism^{7–11} and they all concur in helping cancer cells to escape from apoptosis. These pathways have been investigated in depth and might be inhibited by relatively new classes of anticancer drugs, to contrast the angiogenesis process, such as VEGFR (sunitinib, sorafenib), VEGF directed monoclonal antibodies (bevacizumab), and mTOR (everolimus, temsirolimus) inhibitors^{12–17}. In this contest, the key role of human carbonic anhydrases, a class of metalloproteins that catalyse the reversible conversion of carbon dioxide to bicarbonate and protons^{18–20}, has been outlined. In particular, two membrane isoforms, namely hCA IX and XII, are mainly involved in cancer proliferation and invasion^{21–31}. Not surprisingly, several inhibitors of membrane bounded hCA isozymes, with diverse structures and mechanisms of action, have been designed and investigated so far. In this respect, both synthetic and natural coumarin derivatives have already demonstrated to possess high selectivity and activity towards specific hCA isozymes^{32–36}. Moreover, their interaction and binding mode on this class of metalloenzymes have been investigated in depth^{37,38}. Besides, it should be considered that coumarins have been reported to interact with several cancer





druggable targets. In particular, coumarin derivatives have shown a variety of biological activities such as CK2 inhibitors³⁹, EGFR⁴⁰, PI3K-AKT-mTOR signalling inhibitors^{41–43}. Furthermore, their anti-cancer potential, tumour targets, diverse mechanisms of action as well as their advantages and disadvantages have been recently reviewed⁴⁴. In continuation with our previous work and prompted by these considerations, to further explore the influences of structural modifications on the coumarin and psoralene core on the activity and selectivity towards membrane-bound hCA isozyme, we have designed and synthesised a small library of methyl-2-[4-methyl-2-oxo-7-(2-oxo-2-arylethoxy)-8-propylchromen-3-yl]acetate and 2-(5-methyl-7-oxo-3-aryl-9-propyl-7H-furo[3,2-g]chromen-6-yl)acetic acid derivatives where a propyl group in the position 8 or 9 has been introduced compared to the previously synthesised derivatives.


Methods

Materials and apparatus

Starting materials and reagents were obtained from commercial suppliers and were used without purification. All melting points were determined on a Stuart SMP11 melting points apparatus and are uncorrected. Melting points, the yield of reactions, and analytical data of derivatives **EMAC10157a-b-d-g** and **EMAC10160a-b-d-g** are reported in Table 1.

¹H-NMR and ¹³C-NMR spectra (Table 2) were registered on a Bruker AMX 400 MHz (chemical shifts in δ values) operating at

CONTACT Claudiu T. Supuran  claudiu.supuran@unifi.it  Dipartimento NEUROFARBA, Sezione di Scienze Farmaceutiche, Università degli Studi di Firenze, Via U. Schiff 6, Sesto Fiorentino 50019, Italy; Elias Maccioni  maccione@unica.it  Department of Life and Environmental Sciences, University of Cagliari, A Building-Cittadella Universitaria, s.p 8 km 0.7, Monserrato 09042, Italy

 Supplemental data for this article can be accessed [here](#).

© 2021 The Author(s). Published by Informa UK Limited, trading as Taylor & Francis Group.

This is an Open Access article distributed under the terms of the Creative Commons Attribution License (<http://creativecommons.org/licenses/by/4.0/>), which permits unrestricted use, distribution, and reproduction in any medium, provided the original work is properly cited.

Table 1. Chemical, analytical, and physical data of derivatives **EMAC10157 a-b-d-g** and **EMAC10160 a-b-d-g**.

Compound	R	C, %; H, %		M.P., °C	Yield, % ^a	Aspect
		Calc.	Found			
EMAC10157a	4-CH ₃	C, 71.07; H, 6.20	C, 71.10; H, 6.19	132–133	80	White crystals
EMAC10157b	4-OCH ₃	C, 68.48; H, 5.98	C, 68.74; H, 5.97	127–130	89	Pale brown crystals
EMAC10157d	4-F	C, 67.60; H, 5.44	C, 67.79; H, 5.45	164–166	90	White crystals
EMAC10157g	4-C ₆ H ₅	C, 74.36; H, 5.82	C, 74.55; H, 5.45	138–140	71	White crystals
EMAC10160a	4-CH ₃	C, 74.24; H, 5.98	C, 74.19; H, 5.99	226–229	98	Grey crystals
EMAC10160b	4-OCH ₃	C, 71.41; H, 5.75	C, 71.68; H, 5.76	202–205	97	Green crystals
EMAC10160d	4-F	C, 70.58; H, 5.18	C, 70.30; H, 5.16	135–139	92	Grey crystal
EMAC10160g	4-C ₆ H ₅	C, 77.24; H, 5.62	C, 77.52; H, 5.60	248–250	97	Pale brown crystal

^aYields are referred to the last step of the synthetic pathway.

Table 2. ¹H NMR and ¹³C NMR data of derivatives **EMAC10157a-b-d-g** and **EMAC10160a-b-d-g**.

Compound	¹ H NMR and ¹³ C NMR δ (ppm)
EMAC10157a	¹ H NMR (400 MHz, DMSO) δ 7.93 (d, 2H, <i>J</i> = 8), 7.61 (d, 1H, <i>J</i> = 9.2), 7.39 (d, 2H, <i>J</i> = 8), 7.00 (d, 1H, <i>J</i> = 8.8), 5.74 (s, 2H), 3.68 (s, 2H), 3.62 (s, 3H), 2.83–2.79 (m, 2H), 2.41 (s, 3H), 2.37 (s, 3H), 1.64–1.55 (m, 2H), 0.95–0.91 (t, 3H). ¹³ C NMR (100 MHz, DMSO) δ 193.70, 170.64, 160.88, 158.24, 150.61, 149.69, 144.37, 131.78, 129.34 (2C), 127.96 (2C), 123.92, 116.97, 115.87, 113.65, 108.77, 70.55, 51.82, 32.37, 24.34, 21.70, 21.22, 15.10, 13.96.
EMAC10157b	¹ H NMR (400 MHz, DMSO) δ 8.01 (d, 2H, <i>J</i> = 8.8), 7.61 (d, 1H, <i>J</i> = 8), 7.09 (d, 2H, <i>J</i> = 8), 6.98 (d, 1H, <i>J</i> = 8), 5.70 (s, 2H), 3.86 (s, 3H), 3.68 (s, 2H), 3.62 (s, 3H), 2.82–2.79 (m, 2H), 2.36 (s, 3H), 1.64–1.55 (m, 2H), 0.95–0.91 (t, 3H). ¹³ C NMR (100 MHz, DMSO) δ 192.48, 170.64, 163.61, 160.89, 150.60, 149.69, 130.23 (2C), 127.15, 123.90, 116.96, 115.84, 114.05 (2C), 113.61, 108.76, 70.35, 55.60, 51.81, 32.36, 24.34, 21.70, 15.09, 13.96.
EMAC10157d	¹ H NMR (400 MHz, DMSO) δ 8.13–8.10 (m, 2H), 7.62 (d, 1H, <i>J</i> = 9.2), 7.45–7.40 (m, 2H), 7.03 (d, 1H, <i>J</i> = 9.2), 5.77 (s, 2H), 3.68 (s, 2H), 3.62 (s, 3H), 2.83–2.79 (m, 2H), 2.37 (s, 3H), 1.64–1.55 (m, 2H), 0.95–0.91 (t, 3H). ¹³ C NMR (100 MHz, DMSO) δ 192.90, 170.65, 166.59, 164.08, 160.89, 158.15, 150.60, 149.70, 131.01 (2C), 123.94, 116.98, 116.01, 115.91 (2C), 113.70, 108.79, 70.55, 51.82, 32.36, 24.33, 21.70, 15.10, 13.95.
EMAC10157g	¹ H NMR (400 MHz, DMSO) δ 8.12 (d, 2H, <i>J</i> = 8.4), 7.88 (d, 2H, <i>J</i> = 8.4), 7.78 (d, 2H, <i>J</i> = 7.2), 7.65–7.61 (m, 1H), 7.53 (t, 2H, <i>J</i> = 7.2), 7.45 (t, 1H, <i>J</i> = 7.2), 7.06–7.02 (m, 1H), 5.82 (s, 2H), 3.68 (s, 2H), 3.62 (s, 3H), 2.85–2.81 (m, 2H), 2.37 (s, 3H), 1.64–1.58 (m, 2H), 0.96–0.92 (t, 3H). ¹³ C NMR (100 MHz, DMSO) δ 193.78, 170.63, 160.88, 158.22, 150.62, 149.68, 145.17, 138.77, 133.07, 129.10 (2C), 128.61 (2C), 127.02 (2C), 126.96 (2C), 123.94, 116.99, 115.90, 113.68, 108.81, 73.94, 70.69, 51.81, 32.37, 24.37, 21.73, 15.11, 13.98.
EMAC10160a	¹ H NMR (400 MHz, DMSO) δ 12.47 (bs, 1H), 8.41 (s, 1H), 8.03 (s, 1H), 7.69 (d, 2H, <i>J</i> = 8), 7.34 (d, 2H, <i>J</i> = 7.6), 3.65 (s, 2H), 3.05–3.01 (m, 2H), 2.51 (s, 3H), 2.38 (s, 3H), 1.78–1.69 (m, 2H), 0.97–0.94 (t, 3H). ¹³ C NMR (100 MHz, DMSO) δ 171.49, 160.72, 154.93, 149.65, 147.36, 143.62, 137.11, 129.72 (2C), 127.82, 127.11 (2C), 122.21, 121.45, 117.83, 116.71, 114.20, 112.93, 32.90, 24.85, 21.93, 20.79, 15.64, 13.83.
EMAC10160b	¹ H NMR (400 MHz, DMSO) δ 12.47 (bs, 1H), 8.37 (s, 1H), 8.01 (s, 1H), 7.73 (d, 2H, <i>J</i> = 8), 7.10 (d, 2H, <i>J</i> = 8.8), 3.82 (s, 3H), 3.65 (s, 2H), 3.04–3.01 (m, 2H), 2.51 (s, 3H), 1.71–1.68 (m, 2H), 0.97–0.94 (t, 3H). ¹³ C NMR (100 MHz, DMSO) δ 171.50, 160.73, 158.92, 154.89, 149.66, 147.34, 143.17, 128.47 (2C), 123.00, 122.31, 121.18, 117.79, 116.66, 114.62 (2C), 114.16, 112.89, 55.17, 32.90, 24.84, 21.92, 15.65, 13.82.
EMAC10160d	¹ H NMR (400 MHz, DMSO) δ 12.47 (bs, 1H), 8.46 (s, 1H), 8.03 (s, 1H), 7.87–7.85 (m, 2H), 7.39–7.35 (m, 2H), 3.65 (s, 2H), 3.05–3.01 (m, 2H), 2.52 (s, 3H), 1.78–1.69 (m, 2H), 0.97–0.94 (t, 3H). ¹³ C NMR (100 MHz, DMSO) δ 171.48, 162.91, 160.68, 160.51, 154.88, 149.67, 147.42, 129.23, 129.23, 127.21, 121.97, 120.59, 117.90, 116.81, 116.16, 115.94, 114.16, 112.98, 32.90, 27.45, 24.84, 21.92, 15.67, 13.82.
EMAC10160g	¹ H NMR (400 MHz, DMSO) δ 12.49 (bs, 1H), 8.54 (s, 1H), 8.13 (s, 1H), 7.92 (d, 2H, <i>J</i> = 8), 7.84 (d, 2H, <i>J</i> = 8.4), 7.75 (d, 2H, <i>J</i> = 7.2), 7.51 (t, 2H, <i>J</i> = 7.2), 7.40 (t, 1H, <i>J</i> = 7.2), 3.67 (s, 2H), 3.07–3.04 (m, 2H), 2.55 (s, 3H), 1.80–1.71 (m, 2H), 0.99–0.95 (t, 3H). ¹³ C NMR (100 MHz, DMSO) δ 171.49, 160.71, 155.01, 149.69, 147.44, 144.21, 139.56, 139.42, 129.93, 129.01 (2C), 127.73 (2C), 127.59, 127.37 (2C), 126.54 (2C), 122.04, 121.13, 117.92, 116.84, 114.35, 113.03, 32.92, 24.88, 21.94, 15.71, 13.85.

400 MHz and 100 MHz, respectively. All samples were measured in DMSO. Chemical shifts are reported referenced to the solvent in which they were measured. Coupling constants *J* are expressed in hertz (Hz). Elemental analyses were obtained on a Perkin–Elmer 240 B microanalyser. Analytical data of the synthesised compounds are in agreement within ±0.4% of the theoretical values. TLC chromatography was performed using silica gel plates (Merck F 254), spots were visualised by UV light.

General procedure for the synthesis of compound **EMAC10157 a-b-d-g** and **EMAC10160 a-b-d-g**

Synthesis of methyl 2-(7-hydroxy-4-methyl-2-oxo-8-propyl-2H-chromen-3-yl)acetate

A mixture of propylresorcinol (1 eq.), dimethylacetylsuccinate (1 eq.) and sulphuric acid 98% (2.8 eq.) was vigorously stirred at room temperature. The progression of the reaction was monitored by TLC, using ethyl acetate/n-hexane 2:1. After 30 min a

homogeneous sticky solid was obtained which was dissolved in methanol and poured into ice water. The mixture was stirred until ice melting and then filtered off to obtain a light yellow solid. The crude product was washed with ethyl ether giving a white powder that was crystallised from methanol.

Synthesis of methyl-2-[4-methyl-2-oxo-7-(2-oxo-2-arylethoxy)-8-propylchromen-3-yl]acetate (**EMAC 10157 a-b-d-g**)

A hot solution of methyl 2-(7-hydroxy-4-methyl-2-oxo-8-propyl-2H-chromen-3-yl)acetate (1 eq.) in dry acetone was treated with K₂CO₃ (2.5 eq.), stirred vigorously, and treated with the appropriate α-haloketone (1 eq.). The reaction mixture was heated to reflux and stirred for 1–5 h (course of the reaction monitored by TLC using ethyl acetate/n-hexane 5:1). When the reaction was completed, it was cooled at 0 °C and the solution acidified with HCl conc. The resulting precipitate was filtered off and crystallised if necessary.

Synthesis of 2-(5-methyl-7-oxo-3-aryl-9-propyl-7H-furo[3,2-g]chromen-6-yl)acetic acid (EMAC10160 a-b-d-g)

A solution or suspension of coumarin (1 eq., **EMAC10157 a-b-d-g**) in propan-2-ol was treated with NaOH solution (4 eq., 1N). The reaction mixture was heated for 3–4 h, obtaining a dark solution. The solution was cooled to room temperature and poured into ice water. Concentrated HCl was added to the solution, obtaining a suspension that was filtered and crystallised.

Analytical and spectral data of compounds **EMAC10157 a-b-d-g** and **EMAC10160 a-b-d-g** are reported in Tables 1 and 2. $^1\text{H-NMR}$ and $^{13}\text{C-NMR}$ spectra are reported in Supplementary material (Figures S1–S16).

Biological activity

Carbonic anhydrase inhibition assay

The CA catalysed CO_2 hydration/inhibition was measured by using a stopped-flow instrument (Applied Photophysics, Oxford, U.K.) as the method described earlier⁴⁵. Initial rates of the CA-catalysed CO_2 hydration reaction were followed for 10–100 s. The CO_2 concentrations ranged from 1.7 to 17 mM for the determination of the inhibition constants. For each inhibitor, at least six traces of the initial 5–10% of the reaction were used for assessing the initial velocity. The uncatalyzed rates were subtracted from the total observed rates. Stock solutions of inhibitors (10 mM) and dilutions up to 0.01 nM were prepared in distilled-deionized water. Inhibitor and enzyme solutions were preincubated together for 15 min at room temperature prior to assay, in order to allow for the formation of the E–I complex. The inhibition constants were obtained by non-linear least-squares methods using PRISM 3 as reported earlier, and represent the mean from at least three different determinations^{46–48}. hCA I, hCA II, hCA IX (catalytic domain), and hCA XII (catalytic domain) were recombinant proteins produced in-house using our standardised protocol and their concentration in the assay system was in the range of 3–10 nM (and even lower for highly effective, sub-nanomolar inhibitors)^{46–48}.

Molecular modelling

Ligand preparation

The ligands were built using the Maestro GUI⁴⁹. The most stable conformation has been determined by molecular mechanics conformational analysis performed by MacroModel software version 9.2⁵⁰. using the Merck Molecular Force Fields (MMFFs)⁵¹ and GB/SA water implicit solvation model⁵², Polak–Ribier Conjugate Gradient (PRCG) method, 5000 iterations, and a convergence criterion of 0.05 kcal/(mol Å). All the other parameters were left as default.

Protein preparation

The coordinates for hCA isoforms enzymes were taken from the RCSB Protein Data Bank⁵³ (PDB codes 3k34⁵⁴, for isoform II; 5fl4⁵⁵, for isoform IX and 5msa, for isoform XII). The proteins were prepared by using the Maestro Protein Preparation Wizard⁴⁹. Original water molecules were removed.

Docking protocol

Molecular docking studies were performed using QMPL workflow protocol⁵⁶. Grids were defined around the refined structure by centring on crystallised ligands. The other settings were left as default.

Post docking protocol

To better consider, the induced fit phenomena, the most energy favoured generated complexes were fully optimised with the OPLS2005 force field in GB/SA implicit water. The optimisation process was performed setting 10,000 steps interactions up to the derivative convergence criterion equal to 0.05 kJ/(molÅ). The resulting complexes were considered for the binding modes graphical analysis with Pymol⁵⁷ and Maestro.

Results and discussion

As a continuation of our ongoing research in the field of carbonic anhydrase and anticancer agents^{58–62} we have synthesised a new series of methyl-2-[4-methyl-2-oxo-7-(2-oxo-2-arylethoxy)-8-propylchromen-3-yl]acetate and 2-(5-methyl-7-oxo-3-aryl-9-propyl-7H-furo[3,2-g]chromen-6-yl)acetic acid to evaluate their activity and selectivity towards hCA isozymes and to gain information on their structure-activity relationships. The compounds are reported as **EMAC10157 a-b-d-g** and **EMAC10160 a-b-d-g** and their structures are illustrated in Figure 1.

All the synthesised compounds show a propyl substituent in the position 8 or 9 of the coumarin and psoralen nucleus, respectively. As in previously reported derivatives, a methylene carboxylic group was placed in position 3 of the chromene which may lead to the formation of a bidentate chelator of the Zn^{2+} ion in the catalytic pocket, due to the hCA esterase activity^{32,34,63} on the dihydropyranone ring, as illustrated in Figure 2.

The synthesis of the new derivatives is reported in Scheme 1. It consists of the H_2SO_4 mediated Pechman condensation of dimethylacetyl succinate and 2-propylresorcinol at room temperature in solvent-free conditions, followed by a Williamson reaction of the phenolic group in the position 7 of the chromene ring with the appropriate α -halo ketone in dry acetone and K_2CO_3 , to generate the asymmetric ether which will lead to the furocoumarin formation by intramolecular electrophilic substitution, mediated by refluxing in NaOH 1 N water solution.

EMAC10157 a-b-d-g and **EMAC10160 a-b-d-g** were characterised employing analytical and spectroscopic methods and the results are summarised in Tables 1 and 2. Compounds were then submitted to enzymatic evaluation towards hCA I, II, IX, and XII. The results are reported in Table 3. Interestingly, none of the new EMAC derivatives exhibited any inhibition activity towards hCA I and II isozymes. On the contrary, all of them are submicromolar inhibitors of the hCA membrane isoforms IX and XII. This behaviour is in agreement with our previous findings and with the generally observed selectivity profile of coumarin derivatives^{32,33,35,37,38,63}.

Within the tested compounds, **EMAC10157** series was the most active towards the hCA IX and XII isoforms. Therefore, its mechanism of action was investigated in more detail by docking

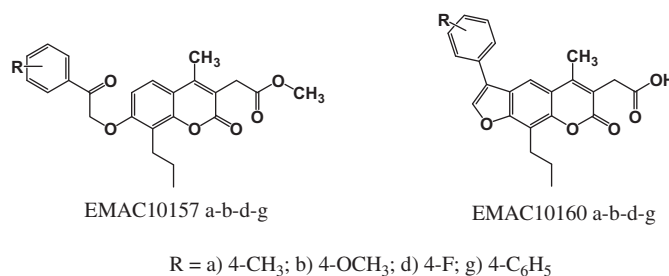


Figure 1. Newly synthesised coumarin and psoralen derivatives.

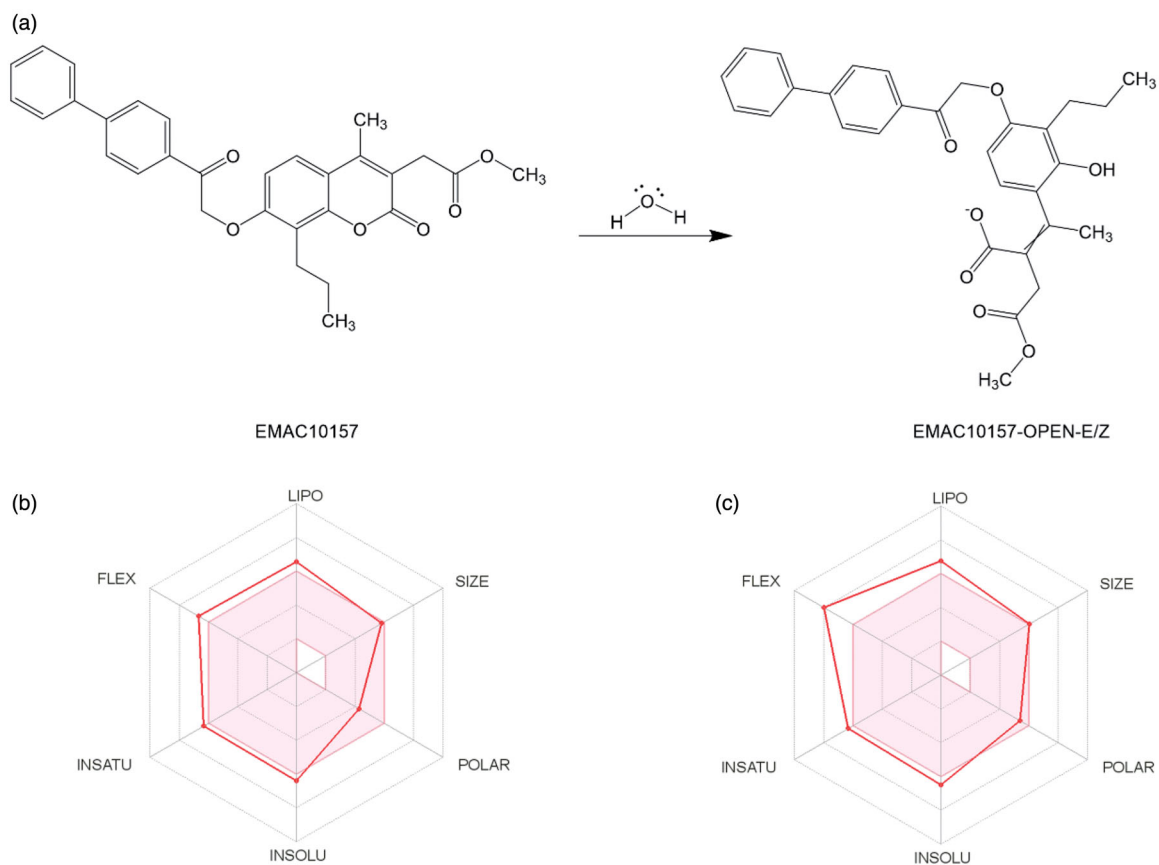
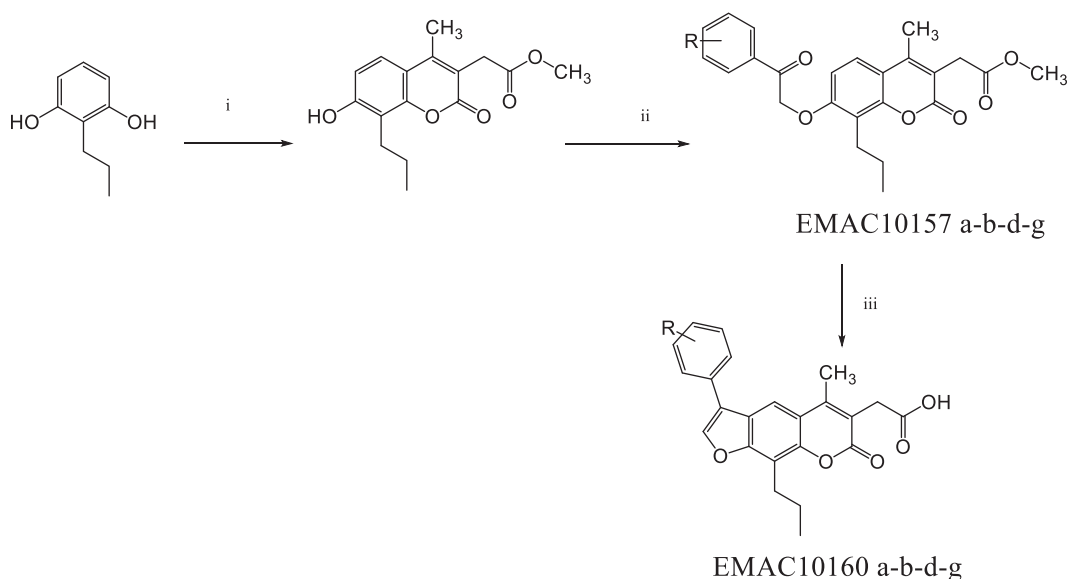


Figure 2. (a) Esterase activity of carbonic anhydrase on compound **EMAC10157g**³⁴. (b, c) Oral bioavailability radar profile.



Scheme 1. Synthetic pathway to compounds **EMAC10157 a-b-d-g** and **EMAC10160 a-b-d-g**. Reagents and conditions: (i) dimethylacetylsuccinate, H₂SO₄ 98% R.T.; (ii) α -halogeno arylketone, dry acetone, K₂CO₃, reflux; (iii) NaOH 1 N, reflux.

experiments followed by energy minimisation of the obtained complexes.

In particular, considering that an interesting hCA esterase mediated inhibition mechanism was recently reported for coumarin derivatives^{32,33,63}, we firstly investigated this aspect. Hence, the most promising compound, **EMAC10157g**, was submitted to docking experiments to evaluate if the dihydropyranone ring of

the chromene moiety could reach the bottom of the catalytic cavity of hCA II, IX and XII and, therefore, be hydrolysed by the Zn²⁺ activated water molecule, which acts as a very potent nucleophile (Figure 2(a)).

Confirming the selectivity profile already observed in previously investigated analogues docking experiment in hCA II enzyme showed that the **EMAC10157g** tail is too bulky to access hCA II

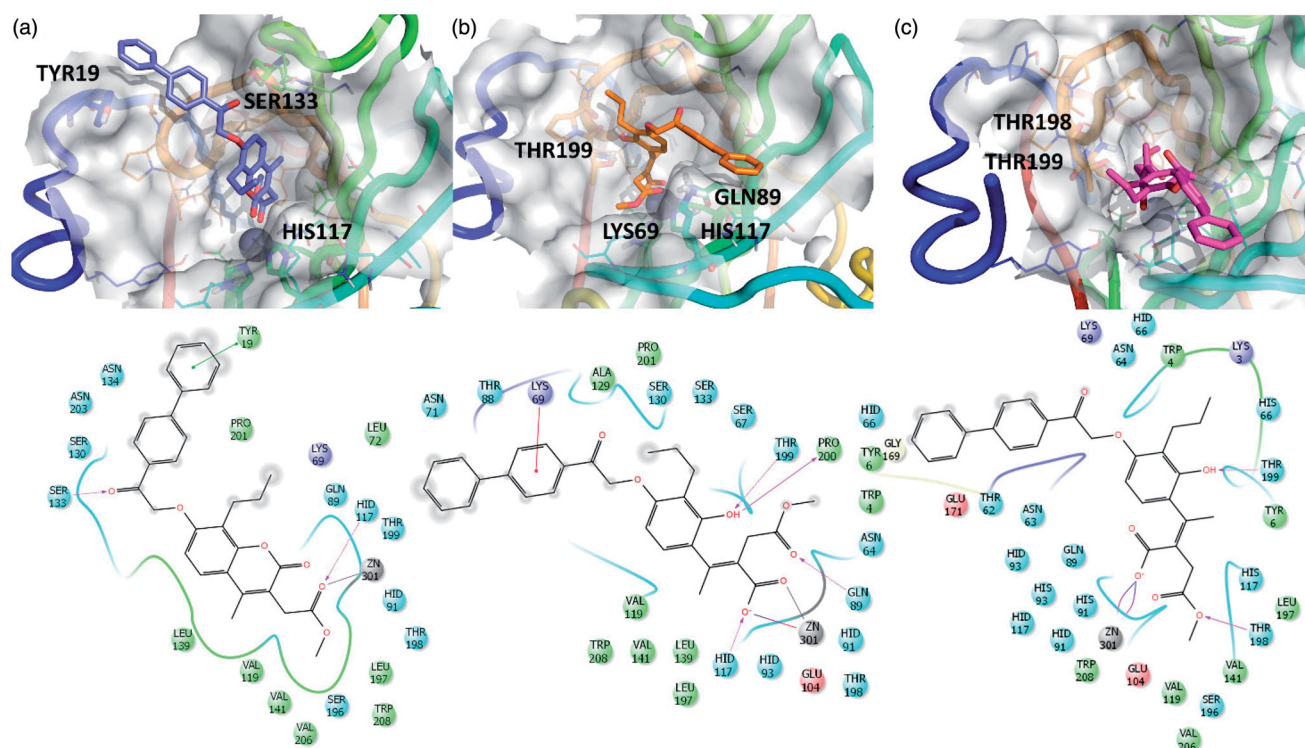


Figure 4. 3D representation of the putative binding mode obtained by docking experiments. (a) hCA-XII – EMAC10157g, (b) hCA-XII – EMAC10157g-openE, and (c) CA-XII – EMAC10157g-openZ and the relative 2D representation of the complexes stabilising interactions with the binding site residues.

formed carboxylate moiety and the methyl ester with the surrounding residues in the catalytic site.

The Y shape of the compound, with propyl and -biphenyl-2oxoethoxy moiety being the arms, helps to maintain the selectivity but, ultimately, decreases the activity, compared to previously investigated psoralens³².

Biphenyl moiety accommodation is well tolerated due to the wide cavity exposed to the solvent, as shown by other hCA inhibitors with bulky tails. In fact, the interactions between this group with adjacent hydrophobic residues stabilise the complexes.

In summary, the computational methods helped to rationalise the good activity of the investigated compound towards the hCA IX and hCA XII isoform and to suggest a reasonable mechanism of action that could be further investigated to be confirmed. If verified, this compound can be considered as a new prodrug candidate with acceptable oral bioavailability properties (Figure 2(b)), and with good drug-like properties. Nevertheless, considering the encouraging predicted ADME properties⁶⁴ and the activity data, we are further optimising this scaffold.

Conclusions

We have designed and synthesised a series of *methyl-2-[4-methyl-2-oxo-7-(2-oxo-2-arylethoxy)-8-propylchromen-3-yl]acetate* and *2-(5-methyl-7-oxo-3-aryl-9-propyl-7H-furo[3,2-g]chromen-6-yl)acetic acid*, and evaluate their activity on hCA I, II, IX, and XII isozymes. As a confirmation of the literature reported chromene derivatives selectivity profile, none of the investigated compounds was able to inhibit the off-target I and II isoforms of hCA. On the contrary, they all inhibit the membrane isozymes hCA IX and XII and further corroborate the reported data on chromene derivatives. Considering the acceptable ADME prediction profile and the high potential of coumarin derivatives, not only as hCA selective inhibitors but also as potential multitarget anticancer agents, these data

prompted us to further investigate this scaffold to optimise both the activity and the isozyme selectivity.

Acknowledgements

The authors wish to acknowledge the “Ufficio Valorizzazione dei Risultati della Ricerca” of Sardegna Ricerche Technological Park, Pula (CA) – Italy. The authors also acknowledge the PRIN 2017 research project “Novel anticancer agents endowed with multi-targeting mechanism of action” (201744BN5T).

Disclosure statement

No potential conflict of interest was reported by the author(s).

ORCID

Rita Meleddu <http://orcid.org/0000-0003-1629-7454>

Elias Maccioni <http://orcid.org/0000-0003-2175-2802>

Francesco Ortuso <http://orcid.org/0000-0001-6235-8161>

Andrea Angeli <http://orcid.org/0000-0002-1470-7192>

Stefano Alcaro <http://orcid.org/0000-0002-0437-358X>

Claudiu T. Supuran <http://orcid.org/0000-0003-4262-0323>

Simona Distinto <http://orcid.org/0000-0003-1620-6225>

References

- Li S-S, Lian Y-F, Huang Y-L, et al. Overexpressing PLOD family genes predict poor prognosis in gastric cancer. *J Cancer* 2020;11:121–31.
- Hoxhaj G, Manning BD. The PI3K-AKT network at the interface of oncogenic signalling and cancer metabolism. *Nat Rev Cancer* 2020;20:74–88.

3. Li Z, You Q, Zhang X. Small-molecule modulators of the hypoxia-inducible factor pathway: development and therapeutic applications. *J Med Chem* 2019;62:5725–49.
4. Ferreira BI, Lie MK, Engelsen AST, et al. Adaptive mechanisms of resistance to anti-neoplastic agents. *MedChemComm* 2017;8:53–66.
5. Krzykawska-Serda M, Miller RC, Elas M, et al. Correlation between hypoxia proteins and EPR-detected hypoxia in tumors. *Adv Exp med Biol* 2017;977:319–325.
6. Huang Y, Lin D, Taniguchi CM. Hypoxia inducible factor (HIF) in the tumor microenvironment: friend or foe? *Sci China Life Sci* 2017;60:1114–24.
7. Lee P, Chandel NS, Simon MC. Cellular adaptation to hypoxia through hypoxia inducible factors and beyond. *Nat Rev Mol Cell Biol* 2020;21:268–83.
8. Xu D, Li DW, Xie J, et al. Effect and mechanism of survivin on hypoxia-induced multidrug resistance of human laryngeal carcinoma cells. *BioMed Res Int* 2019;2019:1–6.
9. Saleh R, Taha RZ, Nair VS, et al. PD-L1 blockade by atezolizumab downregulates signaling pathways associated with tumor growth, metastasis, and hypoxia in human triple negative breast cancer. *Cancers* 2019;11:1050.
10. Maruggi M, Layng FI, Lemos R, Jr., et al. Absence of HIF1A leads to glycogen accumulation and an inflammatory response that enables pancreatic tumor growth. *Cancer Res* 2019;79:5839–48.
11. Chipurupalli S, Kannan E, Tergaonkar V, et al. Hypoxia induced ER stress response as an adaptive mechanism in cancer. *Int J Mol Sci* 2019;20:749.
12. Sanfilippo R, Jones RL, Blay J-Y, et al. Role of chemotherapy, VEGFR inhibitors, and mTOR inhibitors in advanced perivascular epithelioid cell tumors (PEComas). *Clin Cancer Res* 2019;25:5295–300.
13. Saxena AK, Bhuniab SS. Development of VEGFR inhibitors as antiangiogenic agents. *Med Chem Rev* 2016;51:297–310.
14. Berretta M, Rinaldi L, Di Benedetto F, et al. Angiogenesis inhibitors for the treatment of hepatocellular carcinoma. *Front Pharmacol* 2016;7:428–38.
15. Paiva TF, Fonseca de Jesus VH, Marques RA, et al. Angiogenesis-related protein expression in bevacizumab-treated metastatic colorectal cancer: NOTCH1 detrimental to overall survival. *BMC Cancer* 2015;15:643–12.
16. Mishra GP, Doddapaneni BS, Nguyen D, et al. Antiangiogenic effect of docetaxel and everolimus as individual and dual-drug-loaded micellar nanocarriers. *Pharm Res* 2014;31:660–9.
17. Bianco R, Garofalo S, Rosa R, et al. Inhibition of mTOR pathway by everolimus cooperates with EGFR inhibitors in human tumours sensitive and resistant to anti-EGFR drugs. *Br J Cancer* 2008;98:923–30.
18. Mishra CB, Tiwari M, Supuran CT. Progress in the development of human carbonic anhydrase inhibitors and their pharmacological applications: where are we today? *Med Res Rev* 2020;40:2485–565.
19. Domsic JF, Avvaru BS, Kim CU, et al. Entrapment of carbon dioxide in the active site of carbonic anhydrase II. *J Biol Chem* 2008;283:30766–71.
20. Duda DM, Tu C, Fisher SZ, et al. Human carbonic anhydrase III: structural and kinetic study of catalysis and proton transfer. *Biochemistry* 2005;44:10046–53.
21. Nocentini A, Supuran CT. Carbonic anhydrase inhibitors as antitumor/antimetastatic agents: a patent review (2008–2018). *Expert Opin Therap Patents* 2018;28:729–40.
22. Supuran CT. Structure and function of carbonic anhydrases. *Biochem J* 2016;473:2023–32.
23. Supuran CT, Winum JY. Carbonic anhydrase IX inhibitors in cancer therapy: an update. *Future Med Chem* 2015;7:1407–14.
24. Supuran CT. Inhibition of carbonic anhydrase IX as a novel anticancer mechanism. *World J Clin Oncol* 2012;3:98–103.
25. Neri D, Supuran CT. Interfering with pH regulation in tumours as a therapeutic strategy. *Nature Rev Drug Disc* 2011;10:767–77.
26. De Simone G, Supuran CT. Carbonic anhydrase IX: biochemical and crystallographic characterization of a novel antitumor target. *Biochim Biophys Acta* 2010;1804:404–9.
27. Swietach P, Vaughan-Jones RD, Harris AL. Regulation of tumor pH and the role of carbonic anhydrase 9. *Cancer Metast Rev* 2007;26:299–310.
28. Pastorekova S, Parkkila S, Zavada J. Tumor-associated carbonic anhydrases and their clinical significance. *Adv Clin Chem*. 2006;42:167–216.
29. Cecchi A, Hulikova A, Pastorek J, et al. Carbonic anhydrase inhibitors. Design of fluorescent sulfonamides as probes of tumor-associated carbonic anhydrase IX that inhibit isozyme IX-mediated acidification of hypoxic tumors. *J Med Chem* 2005;48:4834–41.
30. Parks SK, Chiche J, Pouysségur J. Disrupting proton dynamics and energy metabolism for cancer therapy. *Nat Rev Cancer* 2013;13:611–23.
31. Angeli A, Carta F, Nocentini A, et al. Carbonic anhydrase inhibitors targeting metabolism and tumor microenvironment. *Metabolites* 2020;10:412.
32. Melis C, Distinto S, Bianco G, et al. Targeting tumor associated carbonic anhydrases IX and XII: highly isozyme selective coumarin and psoralen inhibitors. *ACS Med Chem Lett* 2018;9:725–9.
33. Fois B, Distinto S, Meleddu R, et al. Coumarins from *Magyaris pastinacea* as inhibitors of the tumour-associated carbonic anhydrases IX and XII: isolation, biological studies and in silico evaluation. *J Enzyme Inhibition Med Chem* 2020;35:539–48.
34. Supuran CT. Coumarin carbonic anhydrase inhibitors from natural sources. *J Enzyme Inhibition Med Chem* 2020;35:1462–70.
35. Mancuso F, De Luca L, Angeli A, et al. Synthesis, computational studies and assessment of in vitro inhibitory activity of umbelliferon-based compounds against tumour-associated carbonic anhydrase isoforms IX and XII. *J Enzyme Inhibition Med Chem* 2020;35:1442–9.
36. De Luca L, Mancuso F, Ferro S, et al. Inhibitory effects and structural insights for a novel series of coumarin-based compounds that selectively target human CA IX and CA XII carbonic anhydrases. *Euro J Med Chem* 2018;143:276–82.
37. Temperini C, Innocenti A, Scozzafava A, et al. The coumarin-binding site in carbonic anhydrase accommodates structurally diverse inhibitors: the antiepileptic lacosamide as an example and lead molecule for novel classes of carbonic anhydrase inhibitors. *J Med Chem* 2010;53:850–4.
38. Maresca A, Temperini C, Vu H, et al. Non-zinc mediated inhibition of carbonic anhydrases: coumarins are a new class of suicide inhibitors. *J Am Chem Soc* 2009;131:3057–62.
39. Cozza G, Gianoncelli A, Bonvini P, et al. Urolithin as a converging scaffold linking ellagic acid and coumarin analogues: design of potent protein kinase CK2 inhibitors. *ChemMedChem* 2011;6:2273–86.

40. Yang EB, Zhao YN, Zhang K, et al. Daphnetin, one of coumarin derivatives, is a protein kinase inhibitor. *Biochem Biophys Res Commun* 1999;260:682–5.
41. Liu H, Wang Y, Sharma A, et al. Derivatives containing both coumarin and benzimidazole potently induce caspase-dependent apoptosis of cancer cells through inhibition of PI3K-AKT-mTOR signaling. *Anti-Cancer Drugs* 2015;26:667–77.
42. Mi C, Ma J, Wang KS, et al. Imperatorin suppresses proliferation and angiogenesis of human colon cancer cell by targeting HIF-1 α via the mTOR/p70S6K/4E-BP1 and MAPK pathways. *J Ethnopharmacol* 2017;203:27–38.
43. Park H, Choe H, Hong S. Virtual screening and biochemical evaluation to identify new inhibitors of mammalian target of rapamycin (mTOR). *Bioorg Med Chem Lett* 2014;24:835–8.
44. Wu Y, Xu J, Liu Y, et al. A review on anti-tumor mechanisms of coumarins. *Front Oncol* 2020;10:592853.
45. Khalifah RG. The carbon dioxide hydration activity of carbonic anhydrase. I. Stop-flow kinetic studies on the native human isoenzymes B and C. *J Biol Chem* 1971;246:2561–73.
46. Berrino E, Angeli A, Zhdanov DD, et al. Azidothymidine “Clicked” into 1,2,3-triazoles: first report on carbonic anhydrase-telomerase dual-hybrid inhibitors. *J Med Chem* 2020;63:7392–409.
47. Pacchiano F, Carta F, McDonald PC, et al. Ureido-substituted benzenesulfonamides potently inhibit carbonic anhydrase IX and show antimetastatic activity in a model of breast cancer metastasis. *J Med Chem* 2011;54:1896–902.
48. Bilginer S, Gonder B, Gul HI, et al. Novel sulphonamides incorporating triazene moieties show powerful carbonic anhydrase I and II inhibitory properties. *J Enzyme Inhibition Medi Chem* 2020;35:325–9.
49. Schrödinger LLC.: New York N, USA, 2018.
50. Mohamadi F, Richards NGJ, Guida WC, et al. Macromodel—an integrated software system for modeling organic and bioorganic molecules using molecular mechanics. *J Comput Chem* 1990;11:440–67.
51. Halgren TA. Merck molecular force field. II. MMFF94 van der Waals and electrostatic parameters for intermolecular interactions. *J Comput Chem* 1996;17:520–52.
52. Kollman PA, Massova I, Reyes C, et al. Calculating structures and free energies of complex molecules: combining molecular mechanics and continuum models. *Acc Chem Res* 2000;33:889–97.
53. Berman HM, Westbrook J, Feng Z, et al. The protein data bank. *Nucleic Acids Res* 2000;28:235–42.
54. Behnke CA, Le Trong I, Godden JW, et al. Atomic resolution studies of carbonic anhydrase II. *Acta Crystallogr Sect D, Biol Crystallogr* 2010;66:616–27.
55. Leitans J, Kazaks A, Balode A, et al. Efficient expression and crystallization system of cancer-associated carbonic anhydrase isoform IX. *J Med Chem* 2015;58:9004–9.
56. Chung JY, Hah JM, Cho AE. Correlation between performance of QM/MM docking and simple classification of binding sites. *J Chem Info Model* 2009;49:2382–7.
57. Schrödinger LLC. The PyMOL molecular graphics system. Version 1.7. New York (NY): Schrödinger LLC.
58. Meleddu R, Petrikaite V, Distinto S, et al. Investigating the anticancer activity of isatin/dihydropyrazole hybrids. *ACS Med Chem Lett* 2019;10:571–6.
59. Meleddu R, Distinto S, Cottiglia F, et al. Tuning the dual inhibition of carbonic anhydrase and cyclooxygenase by dihydrothiazole benzenesulfonamides. *ACS Med Chem Lett* 2018;9:1045–50.
60. Melis C, Meleddu R, Angeli A, et al. Isatin: a privileged scaffold for the design of carbonic anhydrase inhibitors. *J Enzyme Inhib Med Chem* 2017;32:68–73.
61. Bianco G, Meleddu R, Distinto S, et al. N-acylbenzenesulfonamide dihydro-1,3,4-oxadiazole hybrids: seeking selectivity toward carbonic anhydrase isoforms. *ACS Med Chem Lett* 2017;8:792–6.
62. Meleddu R, Maccioni E, Distinto S, et al. New 4-[(3-cyclohexyl-4-aryl-2,3-dihydro-1,3-thiazol-2-ylidene)amino]benzenesulfonamides, synthesis and inhibitory activity toward carbonic anhydrase I, II, IX, XII. *Bioorg Med Chem Lett* 2015;25:3281–4.
63. Maresca A, Supuran CT. Coumarins incorporating hydroxy- and chloro-moieties selectively inhibit the transmembrane, tumor-associated carbonic anhydrase isoforms IX and XII over the cytosolic ones I and II. *Bioorg Med Chem Lett* 2010;20:4511–4.
64. Daina A, Michielin O, Zoete V. SwissADME: a free web tool to evaluate pharmacokinetics, drug-likeness and medicinal chemistry friendliness of small molecules. *Sci Rep* 2017;7:42717.